



Stiffening mechanisms in stochastic athermal fiber networks

N. Parvez , J. Merson , and R. C. Picu ^{*}

Department of Mechanical, Aerospace and Nuclear Engineering, Rensselaer Polytechnic Institute, Troy, New York 12180, USA



(Received 4 August 2023; accepted 6 October 2023; published 31 October 2023)

Stochastic athermal networks composed of fibers that deform axially and in bending strain stiffen much faster than thermal networks of axial elements, such as elastomers. Here we investigate the physical origin of stiffening in athermal network materials. To this end, we use models of stochastic networks subjected to uniaxial deformation and identify the emergence of two subnetworks, the stress path subnetwork (SPSN) and the bending support subnetwork (BSSN), which carry most of the axial and bending energies, respectively. The BSSN controls lateral contraction and modulates the organization of the SPSN during deformation. The SPSN is preferentially oriented in the loading direction, while the BSSN's preferential orientation is orthogonal to the SPSN. In nonaffine networks stiffening is exponential, while in close-to-affine networks it is quadratic. The difference is due to a much more modest lateral contraction in the approximately affine case and to a stiffer BSSN. Exponential stiffening emerges from the interplay of the axial and bending deformation modes at the scale of individual or small groups of fibers undergoing large deformations and being subjected to the constraint of rigid cross-links, and it is not necessarily a result of complex interactions involving many connected fibers. An apparent third regime of quadratic stiffening may be evidenced in nonaffinely deforming networks provided the nominal stress is observed. This occurs at large stretches, when the BSSN contribution of stiffening vanishes. However, this regime is not present if the Cauchy stress is used, in which case stiffening is exponential throughout the entire deformation. These results shed light on the physical nature of stiffening in a broad class of materials including connective tissue, the extracellular matrix, nonwovens, felt, and other athermal network materials.

DOI: [10.1103/PhysRevE.108.044502](https://doi.org/10.1103/PhysRevE.108.044502)

I. INTRODUCTION

Many engineering materials and most biological materials have a network of filaments as their main structural component. In rubber, epoxy, and other molecular networks, the filaments are relatively flexible molecules. In the case of the cytoskeleton, the F-actin protein filaments are semiflexible [1–3], i.e., although still thermal in nature, their bending stiffness is larger [4], which entails large persistence length. Other semiflexible molecular networks have been studied, including fibrin [5–7], vimentin [5,8] and neurofilaments [8]. Collagen networks are the main constituent of connective tissue and the extracellular matrix [9,10]. Collagen fibers forming such networks are athermal. Other athermal fibers include cellulose and polymeric fibers in paper, nonwovens, and textiles. Such commonalities unify these seemingly very diverse systems in the broad class of network materials [11].

All networks encountered in nature have stochastic structure. A minimum set of parameters defining the structure includes [11]: the density (total length of fiber per unit volume), ρ ; the mean segment length, l_c , which is related to the number density of cross-links as $\rho_X = \rho/l_c$; and the mean connectivity (number of fibers connected at a cross-link), z . The orientation tensor provides a quantitative description of the degree of alignment, with scalar measure $\langle P_2 \rangle = \frac{1}{2}(3\langle \cos^2\theta \rangle - 1)$ being a convenient measure of alignment relative to a specified direction (θ is the angle

between the end-to-end vector of the respective fiber and the reference direction and $\langle \dots \rangle$ indicates system averaging). In most cases, fibers are not straight, and the crimp parameter (ratio of the end-to-end length to the contour length) may be used to quantify the degree of fiber tortuosity [12]; the persistence length may be used for the same purpose for thermal fibers.

The mechanical behavior of fiber networks is controlled by the properties of the fibers and cross-links, and by the structure of the network [11,13,14]. Semiflexible networks exhibit strong strain stiffening and multiple stiffening regimes when probed in uniaxial tension and in shear. Stiffening is significantly more pronounced than in the case of molecular networks of flexible filaments, such as rubber, at comparable stretch ratios. They also exhibit a large Poisson effect, with effective incremental Poisson ratios that increase during straining to values much larger than the thermodynamic limit of isotropic continua of 0.5 [15–17]. Auxetic behavior is also observed at relatively small strains in densely packed networks of crimped fibers [18,19]. The strong Poisson effect is rooted in the kinematics of fibers, just like the inverse Poynting effect typically observed when testing such networks in shear [20–22]: a normal stress that tends to shrink the material develops when shear is applied. This exceptional property set motivates the interest in identifying the relationship between structural parameters and mechanics in such materials.

The nonlinear response of networks observed in experiments has three regimes [11,23–25]: regime I is linear elastic and is observed at small stretches; regime II is characterized by a power law relation between the tangent stiffness, E_t ,

^{*}Corresponding author: picuc@rpi.edu

and stress, $E_t \sim S^{q_{II}}$ (S stands for the nominal, first Piola-Kirchhoff stress); while regime III is characterized by a similar power function, $E_t \sim S^{q_{III}}$. Collagen tissues and reconstructed collagen, as well as other networks exhibit $q_{II} \approx 1$, which implies exponential stiffening, $S \sim \exp \lambda$ [15,24]. $q_{II} = 3/2$ is reported for actin [4,8] and vimentin networks [15]. $q_{III} = 1/2$ is predicted by the majority of models, e.g., [20,26,27], and is observed in experiments in which this regime can be reached before the onset of failure or damage [6,24].

The physical nature of strain stiffening in semiflexible networks has been debated for almost two decades. The initial thought was that network-scale stiffening is due to the nonlinear axial behavior of fibers (entropic stiffening) [28]. If the network is assumed to deform affinely, fibers are loaded axially, and if their axial response is nonlinear, this property is inherited by the network. Using the wormlike chain (WLC) model [29,30] to capture the effect of pulling thermal fluctuations of semiflexible filaments—a model considered adequate for filaments such as DNA, actin, and other protein fiber networks [31]—stiffening with exponent $q_{II} = 3/2$ can be reproduced [23]. It was later determined that networks with stochastic structure do not deform affinely and fibers are not loaded just in the axial mode [32–34]. It was shown using various types of models that beamlike fibers deform predominantly in the axial and bending modes, while the shear and torsion modes store much less energy and contribute insignificantly to stress production [15,20]. This shifted attention from the fiber scale to the effect of network kinematics on stiffening.

Two lines of thought emerged to explain the two regimes of stiffening. One such perspective [27,35,36] is based on the observation that stress paths (force chains) develop in the network throughout regimes II and III. Stress paths form a subnetwork (SPSN) of fibers carrying high axial strain energy. A stress path is composed of multiple fibers and forms a zigzag path across the network. An athermal stress path taken out from the network and loaded in tension leads to $E_t \sim S^{3/2}$ [37], i.e., a relation identical to that obtained for the thermal filament described by the WLC model [28]. This physical picture implies that the transition between regimes I and II, T_1 , is associated with a shift to axial dominance. An alternate perspective [23,28] is that regime II is entirely bending dominated, and stiffening is associated with the gradual elimination of soft bending modes and is sustained by the pronounced nonaffinity of network kinematics. In this view, transition T_1 between regimes I and II is due to bending buckling of fibers and not to the transition to the axial mode; however, the transition between regimes II and III, T_2 , is assumed to coincide with the shift to axial mode dominance. An attempt was made to associate stiffening in regime II with the inverse Poynting effect and the emergence of the normal stress [38]. This is based on the notion that tensile macroscopic prestress increases the stiffness of a network probed in shear [39,40]. These two perspectives have been compared in [37].

One of the hallmarks of athermal network behavior is the prevalence of exponential stiffening, i.e., $q_{II} = 1$. Most biological tissue, including tendon, skin, the amnion, and the liver capsule strain stiffen exponentially [38,41–43]. This functional form is independent of the network density, pro-

vided the networks deforms nonaffinely [24,38,44]. The same behavior is observed in shear [24,44] and under multiaxial loading conditions [41,45]. In triaxial loading the stress at the transition from regime I to II is smaller than in biaxial loading, which is smaller than measured in uniaxial tests [45]. The presence of crimp has no effect on the functional form of stiffening and q_{II} is independent of the crimp parameter [35,46]. The only effect of increasing fiber tortuosity is to shift the transition to regime II to larger stretches. If a network of fibers made from the same elastic material strain stiffens exponentially, the same network in which the elastic stiffness of fibers is selected from a distribution also stiffens exponentially, with $q_{II} = 1$ [40,47]. This outlines the impressive robustness of exponential stiffening.

In this work we revisit these concepts and address the question of the deformation mode and the mechanism controlling stiffening in regime II. We determine that stiffening is determined by the behavior of individual or small groups of beamlike fibers with constrained relative angles at cross-links subjected to large deformations and rotation. We observe that axial dominance occurs at stretches smaller than those previously reported and largely defines regime II. Hence, the proposed perspective combines elements of current models of stiffening, focusing on individual or small groups of fibers rather than on the large-scale correlated kinematics of fibers forming stress paths. It also demonstrates the stabilizing role of the bending-dominated subnetwork which is not part of the stress paths and its role in defining the onset of regime III.

II. METHODS AND MODELS

Models of athermal cross-linked fibers without embedding matrix are used in this work [26,46]. The fibers are modeled as beams of circular section and diameter d . The cross-links are welded and transmit forces and moments. The relative angle between any pair of fibers coming into a cross-link is fixed. The fiber material is linear elastic with Young's modulus E_f ; the Poisson ratio of the fiber material is irrelevant in this model. Fibers may deform in the axial, bending, shear, and torsional modes. Direct contact between fibers may take place, but it is infrequent when the network is loaded in tension [26].

The model is defined in a cubic domain of edge length L by constructing a Voronoi tessellation based on randomly distributed seed points. The edges of the Voronoi tessellation are retained as fibers. The number density of seed points defines the network density ρ , while the vertices of the tessellation are the network cross-links. The nominal connectivity of this network is $z = 4$. The fiber length (distance between two cross-links) is Poisson distributed and the mean fiber length, l_c , is related to the density as $\rho l_c^2 \approx 1$ [48]. Fibers have no preferential orientation in the initial configuration, are straight, and are modeled using quadratic Timoshenko beam elements. The solution is obtained using the commercial software ABAQUS EXPLICIT, version 2023 [49]. The finite element method solves a numerical representation of the variational form of the equilibrium equations and the solution is the displacement field that minimizes the potential energy. However, the deformation of network materials involves large geometric nonlinearity and the potential for the emergence of local instabilities, and cannot be solved in the static sense

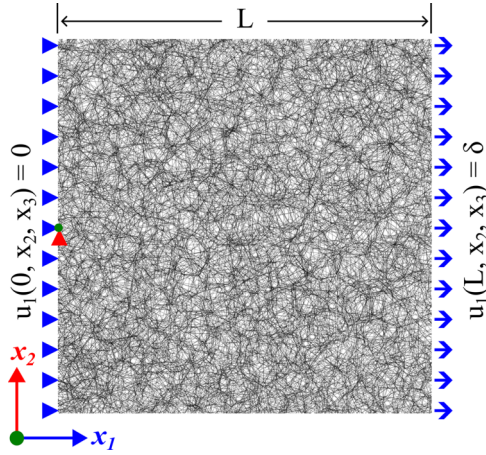


FIG. 1. 2D projection of a three-dimensional (3D) Voronoi-type fiber network model with boundary conditions shown. The 3D domain is cubic with edge length L .

using an implicit formulation, except in the limit of infinitesimal strains. Here we obtain the quasistatic solution using a forward marching integration scheme and adequate damping such as to keep the effect of inertia forces vanishingly small and the kinetic energy smaller than 5% of the total energy. Further details of the method are discussed in [50–52].

Figure 1 shows a model and the boundary conditions applied: the displacement of all nodes at $x_1 = 0$ is zero, $u_1(0, x_2, x_3) = 0$, while that of the nodes at $x_1 = L$ is specified, $u_1(L, x_2, x_3) = \delta$. Therefore, the applied stretch is $\lambda_1 = \lambda = 1 + \delta/L$. Rigid body translations are eliminated by removing the other degrees of freedom of one of the model boundary nodes at $x_1 = 0$. The nodes on the lateral faces are constrained by imposing kinematic ties such that these faces are free to move in the direction orthogonal to the loading direction and remaining planar.

The model size is selected large enough, $L/l_c = 36$, to minimize size effects on the stress-stretch curve [53,54]. Considering six realizations of such models it is inferred that, at each stretch value, the stress has a spread characterized by a coefficient of variation ranging from 4% to 6%.

The discussion is carried out using the nominal stress, \mathbf{S} , unless otherwise specified. Let $S_{11} = S$ be the only nonzero component of the stress in uniaxial deformation. The tangent stiffness is computed as $E_t(\lambda) = dS/d\lambda$, with $E_0 = E_t(1)$ being the small strain stiffness and λ the stretch in the x_1 direction. The total energy is written as the superposition of contributions of the axial, bending, shear, and torsional deformation modes of fibers: $U = U^a + U^b + U^t + U^s$. Since the shear and torsional components are negligible (as observed here and broadly in the literature, e.g., [32,34]), we approximate $U \approx U^a + U^b$. The nominal stress can be written as the superposition of the corresponding stress components: $S = S^a + S^b = (\partial U^a/\partial \lambda + \partial U^b/\partial \lambda)/L^3$, while the tangent stiffness may be also decomposed as $E_t = E_t^a + E_t^b = (\partial S^a/\partial \lambda + \partial S^b/\partial \lambda)$.

The network is characterized by the density, ρ , and fiber diameter, d . The mechanical behavior and the degree of non-affinity of a network are typically discussed in terms of the nondimensional parameter $w = \log_{10} \rho l_b^2$, with $l_b = d/4$ [11].

Networks undergo a nonaffine to affine transition as w increases above a threshold, w_0 [26,32,55,56]. For the type of networks considered here, $w_0 \approx -2$ [57], which corresponds to an aspect ratio of fiber segments, $l_c/d \approx 3$. w also controls the dominant energy storage mode: the bending mode dominates at small strains for $w < w_0$, while the axial mode dominates for $w > w_0$. Hence, the small strain stiffness of the network, E_0 , is proportional to the axial rigidity of fibers, $E_0 \sim E_f d^2$, for $w > w_0$, and to the bending rigidity, $E_0 \sim E_f d^4$, for $w < w_0$ [32,55,56]. In this work we consider two types of networks, with $w = -3.77$ and $w = -2.37$, which are nonaffine and close to the nonaffine-to-affine transition.

III. RESULTS

A. Nonlinear elastic behavior

To make the ideas outlined in the Introduction more specific, we briefly describe the nonlinear behavior of interest. Figure 2(a) shows the stress-stretch curves for the two w values considered, with the three regimes and the respective transitions indicated. The regimes are defined based on the tangent stiffness-stress representation of the data shown in Fig. 2(b). The model predicts $q_{II} \approx 1$ (i.e., exponential stiffening) and $q_{III} \approx 1/2$. As w increases, the range of regime II decreases and eventually vanishes, but q_{III} does not change appreciably. This independence of q_{II} of parameter w is broadly reported in the literature [24,38,44]. Figure 2(c) shows the incremental Poisson ratio, $\nu_i = -d \log \lambda_2 / d \log \lambda$ function of the stretch (with $\lambda_2 = \lambda_3$ since the sample is isotropic at $\lambda = 1$ and transversely isotropic during deformation). As previously reported [15], for $w < w_0$, ν_i increases from an initial value of ~ 0.3 in regime I, to a peak value at the end of regime II, after which it remains constant and then decreases. The peak value is much larger than the isotropic continuum limit of 0.5 due to the large free volume of the network. The volume of the sample decreases almost linearly with λ in regime II and much slower in regime III, as also seen in collagen networks [58,59].

B. Contribution of bending and axial deformation modes

In this section we address the question “what deformation mode controls stiffening in regime II.” Figure 3(a) shows the variation with stretch of the ratios of the axial and bending energies, U^a/U^b ; axial and bending contributions to stress production, S^a/S^b ; and axial and bending contributions to stiffness, E_t^a/E_t^b . Transitions T_1 and T_2 are defined based on the slope of the $E_t(S)$ curve, Fig. 2(b), and the onset of regime III coincides with $U^a/U^b = 1$ for nonaffine networks, $w < w_0$. Stress production becomes axially dominated at smaller stretches, while the stiffness becomes axially dominated even earlier, roughly in the middle of regime II. The bending to axial transition is marked by “BA” in Fig. 3. Hence, axial dominance emerges at stretches smaller than previously reported. Clearly, this transition is not the cause of regime II and of the associated exponent $q_{II} \approx 1$. The data confirm that deformation is bending dominated at the onset of regime II, as proposed in [23], but do not support the idea that it (specifically S and E_t) is bending dominated throughout regime II as claimed in the same references. In the approximately affine

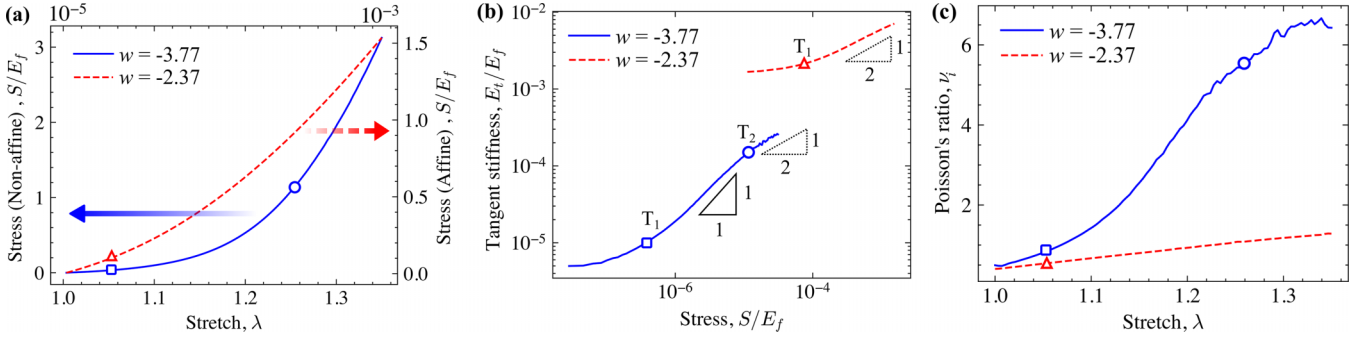


FIG. 2. (a) Nominal stress-stretch, (b) tangent stiffness-stress, and (c) incremental Poisson ratio vs stretch for networks with $w = -3.77$ and $w = -2.37$. The transitions between regimes I and II and between regimes II and III are marked by square and circle symbols, respectively (nonaffine, $w = -3.77$ case), and the transition between regimes I and III in the more affine, $w = -2.37$, case is marked by a triangle.

case of $w = -2.37$, the deformation is axially dominated once regime I ends. In fact, for larger w , axial dominance extends into regime I.

Further, it is useful to compare curves $E_t(S)$, $E_t^a(S^a)$, and $E_t^b(S^b)$ for the nonaffine system ($w = -3.77$), Fig. 4(a). The curves are not aligned in the horizontal direction since the contribution to stress of the two deformation modes is different (see the position of symbols marking the T_1 and T_2 transitions). Both axial and bending modes strain stiffen during regime II, but with different exponents. The exponent of the axial mode is $q_{IIa} \approx 1$, while that of the bending mode is $q_{IIb} \approx 1/2$. At the onset of regime III, the bending mode stops contributing to the incremental stiffness and the bending contribution to stress becomes constant. In regime III the axial mode stiffens with exponent $q_{IIIa} \approx 1/2$ which, due to the axial dominance in this regime, becomes identical to q_{III} .

The behavior of the bending contribution correlates with the incremental Poisson contraction, Fig. 2(c). Once the bending component of stress becomes constant ($E_t^b \rightarrow 0$), incremental ν_i levels off. This suggests that bending provides a background resistance to Poisson contraction, i.e., a bending support subnetwork (BSSN) which controls not only ν_i , but also the rate of formation of the SPSN during regime II.

Figure 4(b) shows similar results for the approximately affine network with $w = -2.37$. The bending contribution to stiffness is constant during regime I and during the beginning

part of regime III; the network enters regime III right after regime I. In regime III, $q_{III} \approx 1/2$ and stiffening is entirely controlled by the axial mode.

C. Stiffening mechanisms

1. Regime II

It is instructive to consider the behavior of periodic networks with unit cells shown in Fig. 5(a). Frames F1 and F2 have welded cross-links and all segments are beams of the same E_f and d . When loaded in tension in direction x_1 , segments AC , AD , BC , and BD bend and stretch to form the equivalent of SPSN, while the bending-dominated segment AB provides resistance to transverse contraction and performs the function of the BSSN. The angles between any pair of fibers merging into a cross-link remain unchanged during deformation.

The tangent stiffness-stress curves (computed based on the nominal stress) for the two structures in Fig. 5(a) are shown in Fig. 5(b). The behavior is similar to that seen in Fig. 2. Regimes I and II are well defined and exponential stiffening ($q_{II} = 1$) is observed. Exponential stiffening persists over a broad range of stretches ($\lambda \approx 1.1, 1.4$) and fiber segment aspect ratios; the independence of the fiber aspect ratio is equivalent to the independence of exponential stiffening on w in stochastic networks. Regime III is not present up to the

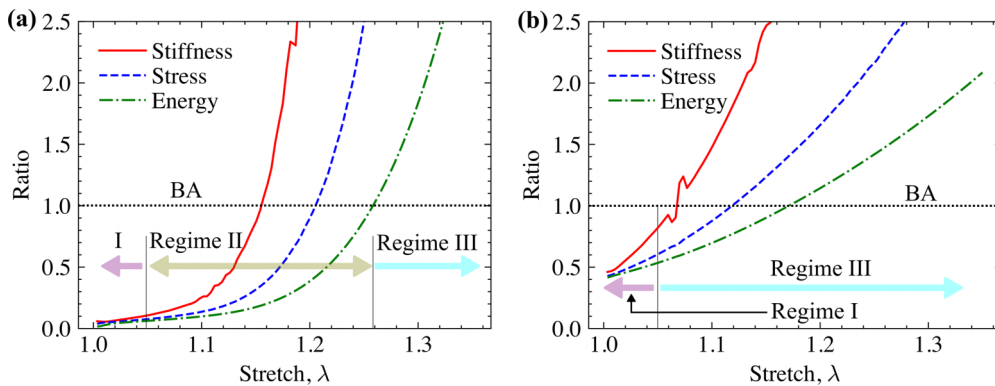


FIG. 3. Variation with the stretch of the ratios of the axial and bending energies, U^a/U^b ; axial and bending contributions to stress production, S^a/S^b ; and axial and bending contributions to stiffness, E_t^a/E_t^b , for (a) $w = -3.77$ and (b) $w = -2.37$. The dotted horizontal line corresponds to the transition from bending to axial mode (BA) for these ratios.

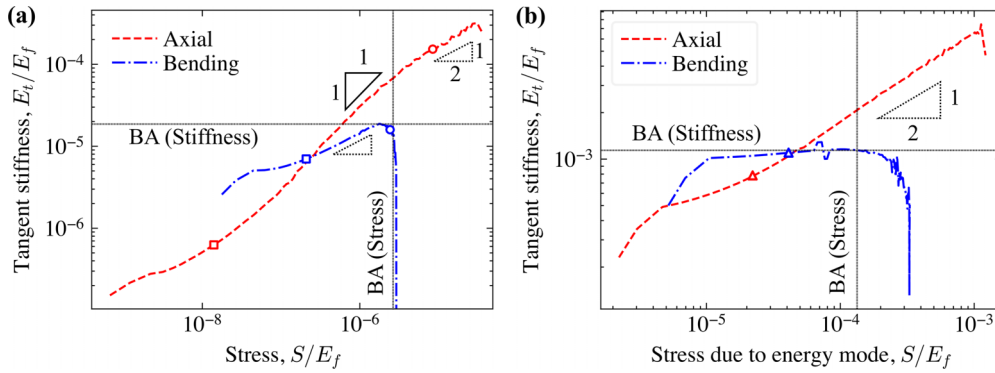


FIG. 4. Stress and stiffness due to axial $E_t^a(S^a)$, and bending, $E_t^b(S^b)$, deformation modes for networks with (a) $w = -3.77$ and (b) $w = -2.37$. Symbols mark the transition between regimes defined based on Fig. 2(b). The horizontal and vertical dotted lines correspond to the bending to axial transitions defined based on the stiffness and stress criteria, respectively.

upper marked point shown in Fig. 5(b), where the structure becomes too distorted to be representative for the network. The stiffness-stress curve computed based on the Cauchy stress is parallel to the curve shown. Since the material is linear, the observed behavior is due to the kinematics of the deformation originating from bending and geometric nonlinearity, conditioned by the nature of the cross-links. The physical picture that emerges is that exponential stiffening results from the interplay of axial and bending modes as fibers undergo large deformations and rotations subjected to the condition of rigidly held angles at cross-links. This also explains the preponderance of this type of stiffening in network materials.

A stress path separated from the stochastic network, which is a zigzag of fiber segments, deforms in a manner similar to that described in Fig. 5 and in Fig. 2 for $w = -3.77$. This relates to the description provided in [27,35,36] in which stiffening is explained based on the pull-out of SPSN. However, here we indicate that considering entire stress paths is unnecessary as each fiber of the structure (or small groups of fibers) exhibits a geometrically nonlinear large deformation behavior compatible with exponential stiffening.

We emphasize the importance of the rotational constraint at cross-links (welded cross-links) for the emergence of exponential stiffening. This is supported by other results from the literature. The opposite limit of the problem is a network

with pin-joint cross-links and truss fibers. A structure of this type and with $z = 4$ is subisostatic. It acquires stiffness upon stretching and exhibits quadratic stiffening rate (slope of $\frac{1}{2}$ in the stiffness-stress plot based on the nominal stress) upon further straining [20]. The bending mode is not engaged in this case. In models in which fiber bending is mimicked using cross-links that penalize the relative rotation of fibers, i.e., both moments and forces are transmitted at cross-links, exponential stiffening emerges [20,60] (if the linear fiber material is replaced with the wormlike chain model, the slope of 1 in the stiffness-stress plot is replaced by $\frac{3}{2}$). This is the case even in fibrous network models of long fibers, each carrying multiple cross-links, in which moments are transmitted at cross-links along each fiber, but not between fibers [24].

It is necessary to discuss at this point the relevance of the welded cross-link model for various network materials. While dwelling on this topic is out of place here, one may observe that (i) nonwovens and networks of spun polymeric fibers are typically cross-linked by merging fibers in contact, a case in which the weld model is appropriate; (ii) F-actin, which is the dominant protein network of the cytoskeleton, is cross-linked by actin binding proteins having an intrinsic nonvanishing stiffness [61]—this may be modeled as a fibrous network connected by rotating springs that transmit moments between fibers; (iii) collagen fibers, which form

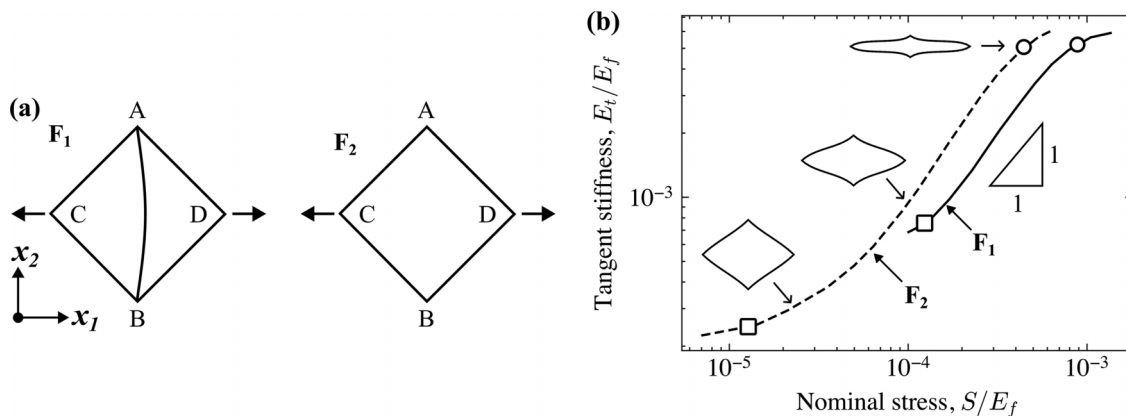


FIG. 5. (a) Unit cells of periodic network of beams, and (b) the corresponding stiffness-stress curves. Deformed configurations of F_2 for a few selected states are shown.

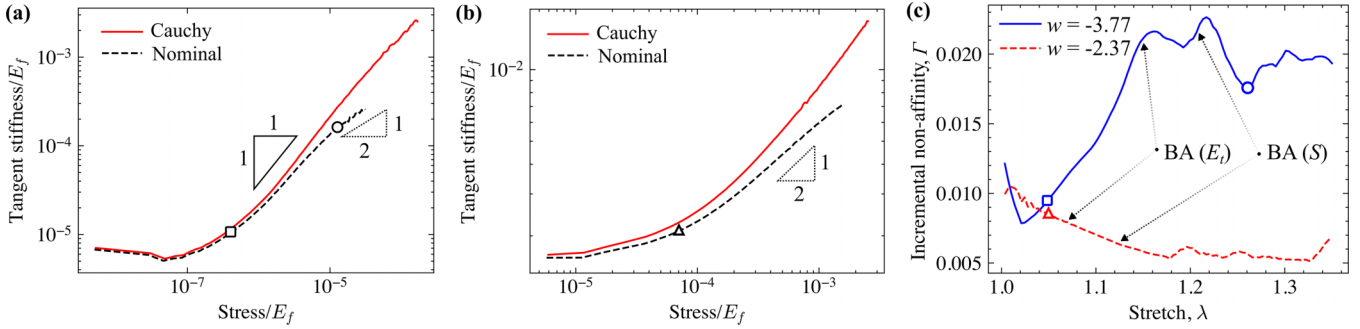


FIG. 6. Tangent stiffness-stress curves for networks with (a) $w = -3.77$ and (b) $w = -2.37$ computed based on the Cauchy and nominal (PK1) stresses. (c) Incremental nonaffinity measure for networks, $\Gamma = \langle |\Delta u_{\text{network}} - \Delta u_{\text{affine}}| \rangle / l_c$, with Δu being the incremental change in displacement field for $w = -3.77$ and $w = -2.37$. The bending to axial transition points (BA) for stress and stiffness (from Fig. 3) are shown in (c).

the extracellular matrix and various connective tissues, have a hierarchical structure and are, in fact, bundles of fibrils held together by covalent bonds—bundles split and merge at the network cross-links and hence moments are transmitted between network segments due to the bending stiffness of the sub-bundles forming each cross-link [62]. While situations in which molecular filaments are cross-linked by fully flexible molecules may be envisioned (a case in which moments are not transmitted between network segments), the prevailing situation appears to be one in which cross-links transmit both forces and moments and restrict fully or partially the relative translation and rotation of the cross-linked segments, as considered in the present models.

2. Regime III

Regime III in nonaffine networks ($w < w_0$) is different from regime III observed in approximately affine networks with larger w , despite the fact that stiffening is described by $q_{\text{III}} = \frac{1}{2}$ in both cases and the deformation is controlled by the axial mode. To shed light on this difference it is useful to replot the tangent stiffness vs stress curves of Fig. 2(b) by using the Cauchy stress. Figure 6(a) shows $E_t(S)$ computed based on the Cauchy and PK1 stresses for the nonaffine case with $w = -3.77$. The slope in regime III for the Cauchy curve is 1, while for the PK1 curve it is $\frac{1}{2}$, as also seen in Fig. 2. The difference is caused by the effect of the transverse contraction, which is considered only when working with the true, Cauchy stress. It results that the real stiffening of nonaffine networks is exponential throughout regimes II and III, while $q_{\text{III}} = \frac{1}{2}$ is an artifact resulting from the use of the nominal stress. This underlines the importance of the mechanism described in Sec. III C, which therefore controls stiffening of nonaffine networks in both regimes II and III.

Figure 6(b) shows similar results for the network with $w = -2.37$. Due to the weak Poisson effect in this case [see Fig. 2(c)], the difference between the curves corresponding to the Cauchy and nominal stresses is minimal and both may be approximated with $q_{\text{III}} \approx 1/2$. The nominal curve departs slightly from the Cauchy curve at the stretch at which $E_t^b \rightarrow 0$ in Fig. 4(b). In this close-to-affine case lateral contraction is minimal and the BSSN is not engaged.

The incremental nonaffinity, computed as the mean of differences between incremental displacement field of network and affine prediction, $\Gamma = \langle |\Delta u_{\text{network}} - \Delta u_{\text{affine}}| \rangle / l_c$, is shown in Fig. 6(c) for both w values. The incremental nonaffinity of the $w = -2.37$ network is much smaller than in the $w = -3.77$ case and decreases monotonically during deformation. The incremental nonaffinity of the $w = -3.77$ network increases in the initial stages of regime II, reaches a plateau when the deformation becomes axially dominated ($E_t^a/E_t^b > 1$), and remains approximately constant throughout the second half of regime II and into regime III. Once again, transition T_2 makes little difference in the incremental nonaffinity as it does in $E_t(S)$ computed based on the Cauchy stress.

This discussion leads to the conclusion that in both non-affine and approximately affine networks deformation has only two regimes: a linear regime at small strains followed by a nonlinear regime. Stiffening is exponential in the case of nonaffine networks and quadratic in the approximately affine case. The weaker stiffening in the affine case is due to the much more modest lateral contraction compared to the nonaffine case.

It is also useful to recall a result from polymer physics where the stiffening rate of the central force network (truss structures with no bending energy storage) was evaluated [63]. The nominal stress in uniaxial loading is given by $S \sim J(\lambda - J/\lambda^2)$, where J is the Jacobian of the transformation. If J is considered independent of λ [see Fig. 2(c) where v_i varies slowly with the stretch], the function $E_t(S)$ decreases continuously for all stretches considered here. This indicates that the interplay of the bending and axial deformation present in beamlike fibers is required to reproduce the type of stiffening observed in semiflexible and athermal networks.

3. Stress path and bending support subnetworks

It is of interest to trace the evolution of the SPSN and BSSN subnetworks throughout the deformation history. The subnetworks are identified as follows: the system is loaded into regime III and the fibers carrying 99% of the axial strain energy are identified as the SPSN. The evolution of the fraction of fibers carrying 99% of the axial, ϕ_a , and bending, ϕ_b , energies at each stretch is shown in Fig. 7(a) for the

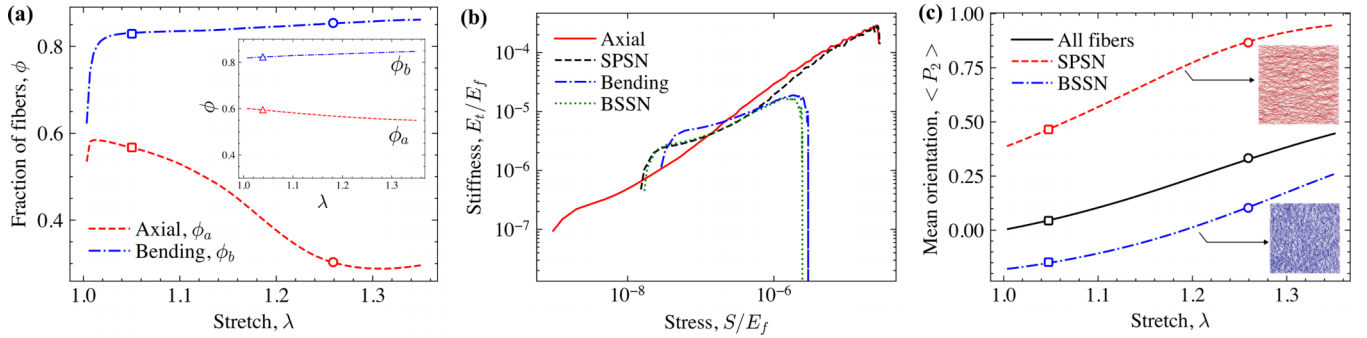


FIG. 7. (a) Fraction of fibers carrying 99% of bending and axial energies at each strain for the network with $w = -3.77$; the inset shows the same fractions for the case with $w = -2.37$. (b) Tangent stiffness-stress curves computed based on the SPSN and BSSN subnetworks along with the corresponding curves computed based on the axial and bending energies, from Fig. 4(a). (c) Average orientation, $\langle P_2 \rangle$, of the SPSN and BSSN subnetworks along with the $\langle P_2 \rangle$ of the entire network. The inset shows these subnetworks traced back to the reference configuration.

$w = -3.77$ case. $\phi_b \approx 0.8$ and is constant during the deformation. ϕ_a decreases rapidly during regime II and becomes constant in regime III to form the SPSN, i.e., $\phi_{\text{SPSN}} = \phi_a$ in regime III. In the case of the network with $w = -2.37$, both ϕ_a and ϕ_b are approximately constant throughout the deformation, as shown in the inset to Fig. 7(a).

BSSN is identified as the set of fibers that carry 99% of the bending energy in regime III but do not belong to SPSN. It results that $\phi_{\text{BSSN}} \approx 0.6$ in the $w = -3.77$ case and 0.33 in the $w = -2.37$ network. Not only are ϕ_{SPSN} and ϕ_{BSSN} constant in regime III, but also the fibers that belong to these subnetworks remain in the respective categories throughout regime III.

To demonstrate the importance of this partition, we consider that the specific fibers identified in regime III as forming the SPSN and BSSN trace their evolution in regimes I and II, and compute their contribution to stress and stiffness. Figure 7(b) shows $E_t(S)$ corresponding to the two subnetworks for $w = -3.77$, i.e., $E_t^{\text{SPSN}}(S^{\text{SPSN}})$ and $E_t^{\text{BSSN}}(S^{\text{BSSN}})$, along with $E_t^a(S^a)$ and $E_t^b(S^b)$. It is observed that $E_t^{\text{SPSN}}(S^{\text{SPSN}}) \approx E_t^a(S^a)$ and $E_t^{\text{BSSN}}(S^{\text{BSSN}}) \approx E_t^b(S^b)$ for most of the stiffening regime, which indicates that the fibers belonging to these subnetworks are critical to the overall network behavior.

Figure 7(c) shows the orientation, P_2 , computed relative to the loading direction, x_1 , of these two sets of fibers traced throughout the loading history. It is seen that SPSN is composed of fibers that are preferentially oriented along the loading direction and that align faster than the system average during regime II, while in regime III SPSN follows the trend of the system average. Conversely, BSSN is preferentially oriented in the direction orthogonal to the SPSN, which is compatible with the view that BSSN provides a support structure against network collapse in regime II.

These data provide support to the physical picture described above in which the SPSN is axially dominated, preferentially oriented in the loading direction, and controls stiffening throughout the second half of regime II, and in

regime III, while BSSN is bending dominated, it is oriented approximately orthogonal to the loading direction and controls the Poisson contraction.

IV. CONCLUSIONS

Using models of fiber networks, we explore the physical basis of strain stiffening in network materials. Stiffening was previously associated with the formation of the stress path subnetwork. We show that SPSN organization is conditioned by the simultaneous formation of a bending support network (BSSN) which is preferentially oriented in the direction orthogonal to SPSN and to the applied uniaxial tensile load. Although the strain energy is bending dominated as the network stiffens (regime II of the deformation), we provide evidence that the stress and stiffness production become axially dominant at far smaller stretches than previously reported. Based on these data, deformation is axially dominated for most of regime II and throughout regime III. In an attempt to explain the exponential functional form of stiffening, we explore several unit cell models and show that exponential stiffening emerges from the behavior of individual or small groups of fibers, and invoking the complex process of SPSN organization to explain stiffening is not necessary. Further, we show that in regime III stiffening is also exponential if the true, Cauchy stress is considered. This contrasts with the quadratic stiffening reported in the literature for this regime which is observed when the nominal stress is used instead. Finally, we conclude that BSSN controls lateral contraction and is responsible for the shift from exponential to quadratic stiffening observed for affine network materials.

ACKNOWLEDGMENT

This work was supported by the National Institutes of Health (NIH) through Grant No. U01 AT010326-06.

[1] P. A. Janmey, S. Hvidt, J. Lamb, and T. P. Stossel, Resemblance of actin-binding protein/actin gels to

covalently crosslinked networks, *Nature (London)* **345**, 89 (1990).

- [2] R. Tharman, M. M. A. E. Claessens, and A. R. Bausch, Viscoelasticity of isotropically cross-linked actin networks, *Phys. Rev. Lett.* **98**, 088103 (2007).
- [3] B. Hinner, M. Tempel, E. Sackmann, K. Kroy, and E. Frey, Entanglement, elasticity, and viscous relaxation of actin solutions, *Phys. Rev. Lett.* **81**, 2614 (1998).
- [4] M. L. Gardel, J. H. Shin, F. C. MacKintosh, L. Mahadevan, P. Matsudaira, and D. A. Weitz, Elastic behavior of cross-linked and bundled actin networks, *Science* **304**, 1301 (2004).
- [5] P. A. Janmey, U. Euteneuer, P. Traub, and M. Schliwa, Viscoelastic properties of vimentin compared with other filamentous biopolymer networks, *J. Cell Biol.* **113**, 155 (1991).
- [6] I. K. Piechocka, K. A. Jansen, C. P. Broedersz, N. A. Kurniawan, F. C. MacKintosh, and G. H. Koenderink, Multi-scale strain-stiffening of semiflexible bundle networks, *Soft Matter* **12**, 2145 (2016).
- [7] K. A. Jansen, R. G. Bacabac, I. K. Piechocka, and G. H. Koenderink, Cells actively stiffen fibrin networks by generating contractile stress, *Biophys. J.* **105**, 2240 (2013).
- [8] Y.-C. Lin, N. Y. Yao, C. P. Broedersz, H. Herrmann, F. C. MacKintosh, and D. A. Weitz, Origins of elasticity in intermediate filament networks, *Phys. Rev. Lett.* **104**, 058101 (2010).
- [9] G. Rh. Owen, M. J. Kääh, and K. Ito, Scanning electron microscopy examination of collagen network morphology at the cartilage, labrum, and bone interfaces in the acetabulum, *Scanning Microsc.* **13**, 83 (1999).
- [10] J. P. R. O. Orgel, A. Miller, T. C. Irving, R. F. Fischetti, A. P. Hammersley, and T. J. Wess, The *in situ* supermolecular structure of type I collagen, *Structure* **9**, 1061 (2001).
- [11] C. R. Picu, *Network Materials: Structure and Properties*, 1st ed. (Cambridge University Press, Cambridge, 2022).
- [12] Y. B. Yi, L. Berhan, and A. M. Sastry, Statistical geometry of random fibrous networks, revisited: Waviness, dimensionality, and percolation, *J. Appl. Phys.* **96**, 1318 (2004).
- [13] M. Rubinstein and S. Panyukov, Elasticity of polymer networks, *Macromolecules* **35**, 6670 (2002).
- [14] C. P. Broedersz and F. C. MacKintosh, Modeling semiflexible polymer networks, *Rev. Mod. Phys.* **86**, 995 (2014).
- [15] R. C. Picu, S. Deogekar, and M. R. Islam, Poisson's contraction and fiber kinematics in tissue: Insight from collagen network simulations, *J. Biomech. Eng.* **140**, 1 (2018).
- [16] D. Wong, A. Andriyana, B. C. Ang, J. J. L. Lee, E. Verron, and M. Elma, Poisson's ratio and volume change accompanying deformation of randomly oriented electrospun nanofibrous membranes, *Plast., Rubber Compos.* **48**, 456 (2019).
- [17] S. Bancelin, B. Lynch, C. Bonod-Bidaud, G. Ducourthial, S. Psilodimitrakopoulos, P. Dokládal, J.-M. Allain, M.-C. Schanne-Klein, and F. Ruggiero, *Ex vivo* multiscale quantitation of skin biomechanics in wild-type and genetically-modified mice using multiphoton microscopy, *Sci. Rep.* **5**, 1 (2015).
- [18] D. Rodney, B. Gadot, O. R. Martinez, S. R. du Roscoat, and L. Orgéas, Reversible dilatancy in entangled single-wire materials, *Nat. Mater.* **15**, 72 (2016).
- [19] V. Negi and R. C. Picu, Mechanical behavior of nonwoven non-crosslinked fibrous mats with adhesion and friction, *Soft Matter* **15**, 5951 (2019).
- [20] A. J. Licup, A. Sharma, and F. C. MacKintosh, Elastic regimes of subisostatic athermal fiber networks, *Phys. Rev. E* **93**, 012407 (2016).
- [21] C. O. Horgan and J. G. Murphy, Poynting and reverse Poynting effects in soft materials, *Soft Matter* **13**, 4916 (2017).
- [22] H. Kang, Q. Wen, P. A. Janmey, J. X. Tang, E. Conti, and F. C. MacKintosh, Nonlinear elasticity of stiff filament networks: Strain stiffening, negative normal stress, and filament alignment in fibrin gels, *J. Phys. Chem. B* **113**, 3799 (2009).
- [23] C. Storm, J. J. Pastore, F. C. MacKintosh, T. C. Lubensky, and P. A. Janmey, Nonlinear elasticity in biological gels, *Nature* **435**, 191 (2005).
- [24] A. J. Licup, S. Münster, A. Sharma, M. Sheinman, L. M. Jawerth, B. Fabry, D. A. Weitz, and F. C. MacKintosh, Stress controls the mechanics of collagen networks, *Proc. Natl. Acad. Sci. U. S. A.* **112**, 9573 (2015).
- [25] F. Burla, Y. Mulla, B. E. Vos, A. Aufderhorst-Roberts, and G. H. Koenderink, From mechanical resilience to active material properties in biopolymer networks, *Nat. Rev. Phys.* **1**, 249 (2019).
- [26] M. R. Islam and R. C. Picu, Effect of network architecture on the mechanical behavior of random fiber networks, *J. Appl. Mech.* **85**, 081011 (2018).
- [27] G. Žagar, P. R. Onck, and E. Van Der Giessen, Two fundamental mechanisms govern the stiffening of cross-linked networks, *Biophys. J.* **108**, 1470 (2015).
- [28] F. C. MacKintosh, J. Käs, and P. A. Janmey, Elasticity of semiflexible biopolymer networks, *Phys. Rev. Lett.* **75**, 4425 (1995).
- [29] N. Saitō, K. Takahashi, and Y. Yunoki, The statistical mechanical theory of stiff chains, *J. Phys. Soc. Jpn.* **22**, 219 (1967).
- [30] O. Kratky and G. Porod, Röntgenuntersuchung gelöster fadenmoleküle, *Recl. Trav. Chim. Pays-Bas* **68**, 1106 (1949).
- [31] T. R. Strick, J.-F. Allemand, D. Bensimon, A. Bensimon, and V. Croquette, The elasticity of a single supercoiled DNA molecule, *Science* **271**, 1835 (1996).
- [32] D. A. Head, A. J. Levine, and F. C. MacKintosh, Distinct regimes of elastic response and deformation modes of cross-linked cytoskeletal and semiflexible polymer networks, *Phys. Rev. E* **68**, 061907 (2003).
- [33] H. Hatami-Marbini and R. C. Picu, Scaling of nonaffine deformation in random semiflexible fiber networks, *Phys. Rev. E* **77**, 062103 (2008).
- [34] R. C. Picu, Mechanics of random fiber networks—a review, *Soft Matter* **7**, 6768 (2011).
- [35] P. R. Onck, T. Koeman, T. van Dillen, and E. van der Giessen, Alternative explanation of stiffening in cross-linked semiflexible networks, *Phys. Rev. Lett.* **95**, 178102 (2005).
- [36] G. Žagar, P. R. Onck, and E. Van Der Giessen, Elasticity of rigidly cross-linked networks of athermal filaments, *Macromolecules* **44**, 7026 (2011).
- [37] T. van Dillen, P. R. Onck, and E. Van der Giessen, Models for stiffening in cross-linked biopolymer networks: A comparative study, *J. Mech. Phys. Solids* **56**, 2240 (2008).
- [38] K. A. Jansen, A. J. Licup, A. Sharma, R. Rens, F. C. MacKintosh, and G. H. Koenderink, The role of network architecture in collagen mechanics, *Biophys. J.* **114**, 2665 (2018).
- [39] M. Sheinman, C. P. Broedersz, and F. C. MacKintosh, Actively stressed marginal networks, *Phys. Rev. Lett.* **109**, 238101 (2012).
- [40] H. Hatami-Marbini and M. Rohanifar, Nonlinear mechanical properties of prestressed branched fibrous networks, *Biophys. J.* **120**, 527 (2021).

- [41] H. Chen, X. Zhao, Z. C. Berwick, J. F. Krieger, S. Chambers, and G. S. Kassab, Microstructure and mechanical property of glutaraldehyde-treated porcine pulmonary ligament, *J. Biomech. Eng.* **138**, 061003 (2016).
- [42] W. Buerzle and E. Mazza, On the deformation behavior of human amnion, *J. Biomech.* **46**, 1777 (2013).
- [43] C.-Y. Huang, A. Stankiewicz, G. A. Ateshian, and V. C. Mow, Anisotropy, inhomogeneity, and tension–compression nonlinearity of human glenohumeral cartilage in finite deformation, *J. Biomech.* **38**, 799 (2005).
- [44] S. Motte and L. J. Kaufman, Strain stiffening in collagen I networks, *Biopolymers* **99**, 35 (2013).
- [45] S. Deogekar and R. C. Picu, Strength of stochastic fibrous materials under multiaxial loading, *Soft Matter* **17**, 704 (2021).
- [46] E. Ban, V. H. Barocas, M. S. Shephard, and C. R. Picu, Effect of fiber crimp on the elasticity of random fiber networks with and without embedding matrices, *J. Appl. Mech.* **83**, 041008 (2016).
- [47] E. Ban, V. H. Barocas, M. S. Shephard, and R. C. Picu, Softening in random networks of non-identical beams, *J. Mech. Phys. Solids* **87**, 38 (2016).
- [48] S. Deogekar, Z. Yan, and R. C. Picu, Random fiber networks with superior properties through network topology control, *J. Appl. Mech.* **86**, 081010 (2019).
- [49] M. Smith, ABAQUS/Standard User’s Manual, Version 6.9 (Dassault Systèmes Simulia Corp, Providence, RI, 2009).
- [50] T. Belytschko, W. K. Liu, B. Moran, and K. Elkhodary, *Nonlinear Finite Elements for Continua and Structures* (John Wiley & Sons, New York, 2014).
- [51] J. Frischkorn and S. Reese, A solid-beam finite element and non-linear constitutive modelling, *Comput. Methods Appl. Mech. Eng.* **265**, 195 (2013).
- [52] A. D’Amore, N. Amoroso, R. Gottardi, C. Hobson, C. Carruthers, S. Watkins, W. R. Wagner, and M. S. Sacks, From single fiber to macro-level mechanics: A structural finite-element model for elastomeric fibrous biomaterials, *J. Mech. Behav. Biomed. Mater.* **39**, 146 (2014).
- [53] A. S. Shahsavari and R. C. Picu, Size effect on mechanical behavior of random fiber networks, *Int. J. Solids Struct.* **50**, 3332 (2013).
- [54] J. Merson and R. C. Picu, Size effects in random fiber networks controlled by the use of generalized boundary conditions, *Int. J. Solids Struct.* **206**, 314 (2020).
- [55] J. Wilhelm and E. Frey, Elasticity of stiff polymer networks, *Phys. Rev. Lett.* **91**, 108103 (2003).
- [56] S. Deogekar and R. C. Picu, On the strength of random fiber networks, *J. Mech. Phys. Solids* **116**, 1 (2018).
- [57] N. Parvez and C. R. Picu, Effect of connectivity on the elasticity of athermal network materials, *Soft Matter* **19**, 106 (2022).
- [58] A. Mauri, A. E. Ehret, M. Perrini, C. Maake, N. Ochsenbein-Kölblle, M. Ehrbar, M. L. Oyen, and E. Mazza, Deformation mechanisms of human amnion: Quantitative studies based on second harmonic generation microscopy, *J. Biomech.* **48**, 1606 (2015).
- [59] D. Vader, A. Kabla, D. Weitz, and L. Mahadevan, Strain-induced alignment in collagen gels, *PLoS One* **4**, e5902 (2009).
- [60] A. Sharma, M. Sheinman, K. M. Heidemann, and F. C. MacKintosh, Elastic response of filamentous networks with compliant crosslinks, *Phys. Rev. E* **88**, 052705 (2013).
- [61] D. Boal, *Mechanics of the Cell*, 2nd ed. (Cambridge University Press, Cambridge, 2012).
- [62] V. Negi and R. C. Picu, Mechanical behavior of cellular networks of fiber bundles stabilized by adhesion, *Int. J. Solids Struct.* **190**, 119 (2020).
- [63] J. H. Weiner, *Statistical Mechanics of Elasticity* (Courier Corporation, North Chelmsford, MA, 2012).